Lanthanide-MOFs as Multifunctional luminescence Sensors

Sibo Wang,[a] Bo Sun,[c] Zhongmin Su,*[c] Guohui Hong,[a] Xiao Li,*[bc] Yanling Liu,[d] Qingqing Pan,[c] Jing Sun[c*]

[a] *School of Materials science and Engineering, Changchun University of Science and Technology, Changchun 130022, People's Republic of China.*

[b] *Laboratory of Preparation and Application of Environmental Friendly Materials (Jilin Normal University), Ministry of Education, Changchun, 130103, China.*

[c] *School of Chemistry and Environmental Engineering, Changchun University of Science and Technology, Jilin Provincial Science and Technology Innovation Center of Optical Materials and Chemistry, Jilin Provincial International Joint Research Center of Photofunctional Materials and Chemistry, Changchun, 130022, China.*

[d] *Chemistry and Chemical Engineering, Hainan Normal University, Hainan, 571158, People's Republic of China.*

1. Exprimental

Materials and General Methods: All reagents and solvents employed were commercially available and used without furthe purification. H_6BDPO was synthesized by a modified literature method.[1] Infrared spectra were obtained from KBr pellets in a wavelength ranging from 4000-400 cm^{-1} on a Nicolet 380 FT-IR spectrophotometer and UV-vis absorption was performed on U-3010 spectrophotometer (Hitachi, Japan). Photoluminescence spectra were recorded on a FL-4600 FL spectrophotometer. Powder X-Ray diffraction (PXRD) patterns were acquired on a Siemens D5005 automated diffractometer with Cu Ka (l = 1.5418 Å) radiation. Thermogravimetric analysis (TGA) was conducted on a Perkin-Elmer FLS-920 analyzer heated from ambient temperature to 1000 °C under argon atmosphere at a ramp rate of 5 °C min^{-1}.

Crystallography: Single crystal X-ray diffraction analyses of CUST-623 - CUST-627 were obtained on a Bruker SMART APEX II CCD diffractometer equipped with a graphite monochromator using Mo Kα radiation (λ = 0.71073 Å) at 296 K. A multiscan technique was used to perform adsorption corrections. All of the structures were solved using direct methods and refined using the full matrix least-squares method on F^2 with anisotropic thermal parameters for all non-hydrogen atoms using the SHELXL-97 program.[2] All hydrogen atoms were located in calculated positions and refined isotropically. The crystal data and structure refinement results of CUST-623 - CUST-627 are summarized in Table S1.

Synthesis of $Eu_xTb_{0.02-x}$-MOF: The synthesis of (x=0.002, 0.004, 0.006, 0.008, 0.010, 0.012, 0.014, 0.016, 0.018) are the same as that of CUST-623. Replace $Ln(NO_3)_3 \cdot 6H_2O$ with a mixture of $Eu(NO_3)_3 \cdot 6H_2O$ and $Tb(NO_3)_3 \cdot 6H_2O$, and keep the total mass amount of Eu^{3+} and Tb^{3+} unchanged at 0.02 g. The contents of Eu^{3+} and Tb^{3+} ions in $Eu_xTb_{0.02-x}$-MOF were confirmed using inductively coupled plasma spectroscopy (ICPS) (Table S4).

Preparation of Ln-MOFs@PVA: Disperse 2 g of polyvinyl alcohol (PVA 1788) in 10 ml of cold water for 12 h and heat in 95 °C water bath for 3 h to allow PVA to dissolve sufficiently. Add 2 g MOFs to the cooled PVA solution and stir vigorously to mix well. Finally, put the mixture into the mold to form films.

Luminescence sensing experiment: For the experiments of luminescence sensing, 3 mg of Ln-MOF powders were added into 3.00 mL of $M(NO_3)_x$ (M=Al^+, K^+, Mg^{2+}, Ca^{2+}, Mn^{2+}, Cd^{2+}, Zn^{2+}, Cu^{2+}, Ag^+, Hg^{2+}, Na^+, Fe^{3+}, Pb^{2+}) , KX (X=I^-, Br^-, NO_3^-, Cl^-, CO_3^{2-}, F^-, $C_2O_4^{2-}$, CrO_4^{2-}, $Cr_2O_7^{2-}$, CN^-) or explosives water solutions, sonicated for 30 minutes to obtain the suspensions. When the suspensions were stayed to be stable enough, they can be used for measurements.

2. Computational Details.

The fluorescence quenching was analyzed using the Stern-Volmer equations:[3]

$$(I_0/I) = K_{sv}[M] + 1$$

where I_0 and I are the fluorescence intensity , in the absence and presence of analyte,

respectively, K_{sv} is the Stern-Volmer quenching constant and [M] is the concentration of analyte.

The limit of detection concentration (LOD) was calculated according to the formula:[4]

$$LOD = 3\delta/K_{sv}$$

and δ is the standard deviation of the detection method.

The relative sensitivity is obtained according to the formula:[5]

$$S_r = \frac{(\partial\Delta/\partial T)}{\Delta}$$

Table S1. Crystal data and structure refinement for CUST-623 - CUST-627

	CUST-623	CUST-624	CUST-625	CUST-626	CUST-627
Empirical formula	$C_{18}H_{16}EuN_2O_{14}$	$C_{18}H_{16}N_2O_{14}Tb$	$C_{18}H_{16}GdN_2O_{14}$	$C_{18}H_{16}DyN_2O_{14}$	$C_{18}H_{16}N_2O_{14}Sm$
CCDC No.	2161782	2161779	2161780	2161781	2161783
Formula weight	636.29	643.25	641.58	646.83	634.68
Temperature/K	296.15	296.15	296.15	296.15	296.15
Crystal system	monoclinic	monoclinic	monoclinic	monoclinic	monoclinic
Space group	$P2_1/c$	$P2_1/c$	$P2_1/c$	$P2_1/c$	$P2_1/c$
a/Å	7.0504(10)	7.063(4)	7.016(6)	7.0224(9)	7.0381(6)
b/Å	16.530(3)	16.544(8)	16.367(15)	16.465(2)	16.5007(15)
c/Å	20.371(3)	20.320(10)	20.184(19)	20.263(3)	20.3416(19)
α/°	90	90	90	90	90
β/°	96.489(5)	96.432(7)	96.619(14)	96.353(3)	96.410(2)
γ/°	90	90	90	90	90
Volume/Å^3	2358.9(6)	2359(2)	2302(4)	2328.6(5)	2347.6(4)
Z	4	4	4	4	4
ρ_{calc}g/cm^3	1.792	1.811	1.851	1.845	1.796
μ/mm^{-1}	2.732	3.071	2.955	3.283	2.575
F(000)	1252.0	1260.0	1256.0	1264.0	1248.0

Reflections collected	40864	13569	13628	18140	19201
Data /parameters	4186/329	4273/329	4367/333	5498/350	5664/357
Gof on F^2	1.091	1.063	1.073	1.126	1.079
Final R indexes [I>=2σ(I)]	R_1 = 0.0245, wR_2 = 0.0633	R_1 = 0.0238, wR_2 = 0.0603	R_1 = 0.0263, wR_2 = 0.0694	R_1 = 0.0250, wR_2 = 0.0621	R_1 = 0.0239, wR_2 = 0.0480
Final R indexes [all data]	R_1 = 0.0281, wR_2 = 0.0649	R_1 = 0.0271, wR_2 = 0.0618	R_1 = 0.0314, wR_2 = 0.0723	R_1 = 0.0265, wR_2 = 0.0627	R_1 = 0.0299, wR_2 = 0.0498
R_{int}	0.0406	0.0303	0.0353	0.0207	0.0247

$R_1^a = \Sigma||F_o|-|F_c||/\Sigma|F_o|$, $wR_2^b = [\Sigma[w(F_o^2-F_c^2)^2]/\Sigma[w(F_o^2)^2]]^{1/2}$

Table S2. Selected bond lengths (Å) for CUST-623 - CUST-627

Bond	Angle (°)	Bond	Angle (°)
Eu1-O1[1]	2.460(3)	Eu1-O6	2.463(3)
Eu1-O2	2.506(3)	Eu1-O7	2.326(3)
Eu1-O4	2.452(3)	Eu1-O8[2]	2.543(3)
Eu1-O5[1]	2.551(3)	Eu1-O12[2]	2.406(3)
[1]-2+X,1/2-Y,-1/2+Z; [2]-X,-1/2+Y,1/2-Z			
Bond	**Angle (°)**	**Bond**	**Angle (°)**
Tb1-O2[1]	2.537(3)	Tb1-O5[1]	2.443(2)
Tb1-O3	2.427(3)	Tb1-O6	2.308(2)
Tb1-O4	2.442(3)	Tb1-O7[2]	2.539(3)
Tb1-O5[1]	2.443(2)	Tb1-O8	2.478(3)
[1]-2+X,1/2-Y,-1/2+Z; [2]-1-X,1-Y,1-Z			
Bond	**Angle (°)**	**Bond**	**Angle (°)**
Gd1-O1[1]	2.521(4)	Gd1-O5[2]	2.528(3)
Gd1-O3	2.436(3)	Gd1-O6	2.424(3)
Gd1-O4	2.295(3)	Gd1-O7	2.472(3)
Gd1-O5[2]	2.528(3)	Gd1-O8[1]	2.430(3)
[1]2+X,3/2-Y,1/2+Z; [2]3-X,1-Y,1-Z			
Bond	**Angle (°)**	**Bond**	**Angle (°)**
Dy1-O1[1]	2.520(2)	Dy1-O5[1]	2.426(2)
Dy1-O2	2.295(2)	Dy1-O6	2.523(2)
Dy1-O3	2.408(2)	Dy1-O9	2.367(2)
Dy1-O4	2.418(3)	Dy1-O12	2.416(2)
[1]1-X,-1/2+Y,3/2-Z; [2]-1-X,1-Y,1-Z			
Bond	**Angle (°)**	**Bond**	**Angle (°)**
Sm1-O1[1]	2.5564(18)	Sm1-O5	2.3305(18)
Sm1-O2[2]	2.5481(18)	Sm1-O7[1]	2.4695(18)
Sm1-O3	2.4638(19)	Sm1-O9	2.511(2)
Sm1-O4	2.456(2)	Sm1-O10	2.457(2)
[1]2+X,1/2-Y,1/2+Z; [2]3-X,1-Y,1-Z			

Table S3. Selected angles (º) for CUST-623 - CUST-627

Bond	Angle (°)	Bond	Angle (°)	Bond	Angle (°)
O1[1]-Eu1-O2	77.73(10)	O6-Eu1-O8[2]	138.85(10)	O12[2]-Eu1-O8[2]	52.57(9)
O1[1]-Eu1-O5[1]	51.63(8)	O7-Eu1-O1[1]	136.68(11)	O12[2]-Eu1-O13	76.77(12)

O1^{1}-Eu1-O6	127.36(9)	O7-Eu1-O2	70.94(9)	O13-Eu1-O2	135.89(11)
O1^{1}-Eu1-O8^{2}	74.06(9)	O7-Eu1-O4	72.98(10)	O13-Eu1-O5^{1}	73.21(11)
O1^{1}-Eu1-O13	99.54(11)	O7-Eu1-O5^{1}	135.88(10)	O13-Eu1-O6	70.41(10)
O2-Eu1-O5^{1}	71.16(10)	O7-Eu1-O6	73.43(10)	O12^{2}-Eu1-O4	82.09(11)
O2-Eu1-O8^{2}	143.98(9)	O7-Eu1-O8^{2}	117.39(9)	O12^{2}-Eu1-O5^{1}	148.07(11)
O4-Eu1-O1^{1}	70.97(9)	O7-Eu1-O12^{2}	71.40(9)	O12^{2}-Eu1-O6	103.28(10)
O4-Eu1-O2	76.08(10)	O8^{2}-Eu1-O5^{1}	106.50(9)	O4-Eu1-O13	145.38(10)
O4-Eu1-O5^{1}	117.94(9)	O7-Eu1-O6	73.43(10)	O6-Eu1-O2	76.75(10)
O4-Eu1-O6	142.08(9)	O12^{2}-Eu1-O1^{1}	125.17(10)	O6-Eu1-O5^{1}	76.68(9)

^{1}-2+X,1/2-Y,-1/2+Z; ^{2}-X,-1/2+Y,1/2-Z; ^{3}2+X,1/2-Y,1/2+Z; ^{4}-X,1/2+Y,1/2-Z

Bond	Angle (°)	Bond	Angle (°)	Bond	Angle (°)
O2^{1}-Tb1-O7^{2}	106.30(9)	O5^{1}-Tb1-O7^{2}	73.49(9)	O8-Tb1-O7^{2}	143.79(9)
O3-Tb1-O2^{1}	118.23(9)	O5^{1}-Tb1-O8	77.86(9)	O10^{2}-Tb1-O3	82.43(11)
O3-Tb1-O4	142.32(9)	O6-Tb1-O2^{1}	135.98(9)	O10^{2}-Tb1-O4	103.24(10)
O3-Tb1-O5^{1}	70.93(9)	O6-Tb1-O3	73.20(10)	O10^{2}-Tb1-O5^{1}	125.15(10)
O3-Tb1-O7^{2}	73.60(9)	O6-Tb1-O4	73.60(10)	O10^{2}-Tb1-O7^{2}	52.98(8)
O3-Tb1-O8	76.45(10)	O6-Tb1-O5^{1}	137.02(10)	O10^{2}-Tb1-O8	141.05(9)
O4-Tb1-O2^{1}	76.16(8)	O6-Tb1-O7^{2}	117.53(9)	O10^{2}-Tb1-O13	76.27(11)
O4-Tb1-O5^{1}	127.19(9)	O6-Tb1-O8	71.35(9)	O13-Tb1-O2^{1}	73.04(10)
O4-Tb1-O7^{2}	139.19(10)	O6-Tb1-O10^{2}	71.37(9)	O13-Tb1-O3	144.88(10)
O4-Tb1-O8	76.48(10)	O6-Tb1-O13	123.80(10)	O13-Tb1-O4	70.76(10)
O5^{1}-Tb1-O2^{1}	51.96(8)	O8-Tb1-O2^{1}	71.01(9)	O8-Tb1-O7^{2}	143.79(9)

^{1}-2+X,1/2-Y,-1/2+Z; ^{2}-1-X,1-Y,1-Z; ^{3}2+X,1/2-Y,1/2+Z

Bond	Angle (°)	Bond	Angle (°)	Bond	Angle (°)
O1^{1}-Gd1-O5^{2}	105.93(10)	O4-Gd1-O13	123.69(11)	O8^{1}-Gd1-O7	77.62(11)
O3-Gd1-O1^{1}	76.64(10)	O6-Gd1-O1^{1}	118.11(9)	O12^{2}-Gd1-O3	103.46(11)
O3-Gd1-O5^{2}	139.02(11)	O6-Gd1-O3	141.86(10)	O12^{2}-Gd1-O5^{2}	52.80(10)
O3-Gd1-O7	76.67(11)	O6-Gd1-O5^{2}	74.10(10)	O12^{2}-Gd1-O6	82.15(12)
O4-Gd1-O1^{1}	136.03(10)	O6-Gd1-O7	75.97(11)	O12^{2}-Gd1-O7	140.73(10)
O4-Gd1-O3	73.31(12)	O6-Gd1-O8^{1}	70.94(11)	O12^{2}-Gd1-O8^{1}	125.02(11)
O4-Gd1-O5^{2}	117.85(11)	O7-Gd1-O1^{1}	71.35(10)	O12^{2}-Gd1-O13	76.41(12)
O4-Gd1-O6	72.96(11)	O7-Gd1-O5^{2}	143.80(9)	O13-Gd1-O1^{1}	73.20(10)
O4-Gd1-O7	71.01(11)	O8^{1}-Gd1-O1^{1}	51.75(9)	O13-Gd1-O3	70.75(10)
O4-Gd1-O8^{1}	136.66(12)	O8^{1}-Gd1-O3	127.36(11)	O13-Gd1-O5^{2}	71.13(10)
O4-Gd1-O12^{2}	71.58(11)	O8^{1}-Gd1-O5^{2}	73.72(11)	O8^{1}-Gd1-O7	77.62(11)

^{1}2+X,3/2-Y,1/2+Z; ^{2}3-X,1-Y,1-Z; ^{3}-2+X,3/2-Y,-1/2+Z

Bond	Angle (°)	Bond	Angle (°)	Bond	Angle (°)
O1^{1}-Dy1-O6	106.47(8)	O3-Dy1-O5^{1}	71.09(9)	O9-Dy1-O1^{1}	147.79(9)
O2-Dy1-O1^{1}	135.87(8)	O3-Dy1-O6	74.06(9)	O9-Dy1-O3	82.75(10)
O2-Dy1-O3	73.04(9)	O3-Dy1-O12	142.02(9)	O9-Dy1-O4	77.04(11)
O2-Dy1-O4	124.31(10)	O3-Dy1-O13	75.46(9)	O9-Dy1-O5^{1}	125.30(9)
O2-Dy1-O5^{1}	137.25(9)	O4-Dy1-O1^{1}	72.29(10)	O9-Dy1-O6	53.16(8)
O2-Dy1-O6	117.49(8)	O4-Dy1-O5^{1}	98.43(10)	O9-Dy1-O12	102.87(10)
O2-Dy1-O9	71.11(8)	O4-Dy1-O6	71.45(9)	O9-Dy1-O13	140.65(9)
O2-Dy1-O12	73.52(9)	O4-Dy1-O13	135.89(10)	O12-Dy1-O1^{1}	76.13(8)
O2-Dy1-O13	71.36(8)	O5^{1}-Dy1-O1^{1}	52.09(7)	O12-Dy1-O4	70.64(9)
O3-Dy1-O1^{1}	118.24(8)	O5^{1}-Dy1-O6	73.45(8)	O12-Dy1-O5^{1}	127.35(8)
O3-Dy1-O4	145.50(10)	O5^{1}-Dy1-O13	77.74(9)	O12-Dy1-O6	138.96(9)

^{1}1-X,-1/2+Y,3/2-Z; ^{2}1-X,1/2+Y,3/2-Z; ^{3}-1-X,1-Y,1-Z

Bond	Angle (°)	Bond	Angle (°)	Bond	Angle (°)
O2^{2}-Sm1-O1^{1}	106.52(6)	O5-Sm1-O1^{1}	135.80(7)	O9-Sm1-O1^{1}	71.23(7)
O3-Sm1-O1^{1}	76.82(6)	O5-Sm1-O2^{2}	117.43(6)	O9-Sm1-O2^{2}	143.67(7)
O3-Sm1-O2^{2}	139.11(7)	O5-Sm1-O3	73.37(7)	O10-Sm1-O1^{1}	73.30(8)
O3-Sm1-O7^{1}	127.15(7)	O5-Sm1-O4	72.89(8)	O10-Sm1-O2^{2}	71.73(8)
O3-Sm1-O9	76.84(7)	O5-Sm1-O7^{1}	136.55(7)	O10-Sm1-O3	70.47(8)
O4-Sm1-O1^{1}	117.27(7)	O5-Sm1-O9	70.72(7)	O10-Sm1-O7^{1}	99.55(8)
O4-Sm1-O2^{2}	74.33(7)	O5-Sm1-O10	123.89(8)	O10-Sm1-O9	136.04(9)
O4-Sm1-O3	141.58(8)	O5-Sm1-O11^{2}	71.51(7)	O11^{2}-Sm1-O1^{1}	148.36(7)
O4-Sm1-O7^{1}	70.81(7)	O7^{1}-Sm1-O1^{1}	51.30(6)	O11^{2}-Sm1-O2^{2}	52.42(6)
O4-Sm1-O9	75.14(7)	O7^{1}-Sm1-O2^{2}	74.20(6)	O11^{2}-Sm1-O3	103.68(8)
O4-Sm1-O10	146.07(8)	O7^{1}-Sm1-O9	77.53(7)	O11^{2}-Sm1-O4	82.40(8)

^{1}2+X,1/2-Y,1/2+Z; ^{2}3-X,1-Y,1-Z; ^{3}-2+X,1/2-Y,-1/2+Z

Table S4. The molar ratio of Eu/Tb in compounds produced by ICP.

Sample	The molar of the starting Eu/Tb salt	The molar by ICP analysis
$Eu_{0.002}Tb_{0.018}$-MOF (Eu: Tb=1: 9)	0.002:0.018	0.00223: 0.01777
$Eu_{0.004}Tb_{0.016}$-MOF (Eu: Tb=2: 8)	0.004:0.016	0.00419: 0.01581
$Eu_{0.006}Tb_{0.014}$-MOF (Eu: Tb=3: 7)	0.006:0.014	0.00607: 0.01393
$Eu_{0.008}Tb_{0.012}$-MOF (Eu: Tb=4: 6)	0.008:0.012	0.00811: 0.01189
$Eu_{0.010}Tb_{0.010}$-MOF (Eu: Tb=5: 5)	0.010:0.010	0.01002: 0.00998
$Eu_{0.012}Tb_{0.008}$-MOF (Eu: Tb=6: 4)	0.012:0.008	0.01198: 0.00802
$Eu_{0.014}Tb_{0.006}$-MOF (Eu: Tb=7: 3)	0.014:0.006	0.01392: 0.00608
$Eu_{0.016}Tb_{0.004}$-MOF (Eu: Tb=8: 2)	0.016:0.004	0.01587: 0.00413
$Eu_{0.018}Tb_{0.002}$-MOF (Eu: Tb=9: 1)	0.018:0.002	0.01782: 0.00218

Table S5. Composition, working ranges (K), maximum relative sensitivity values (S_m, % K^{-1}), and the temperature at which Sm is maximum (T_m, K) of luminescent MOF thermometers.

Luminescent thermometer	Range (K)	S_m (% K^{-1})	T_m	Ref.
$Eu_{0.002}Tb_{0.018}$-BDPO	303-423	2.4	423	This work
$Eu_{0.004}Tb_{0.016}$-BDPO	303-423	1.7	423	This work
$Eu_{0.002}Tb_{0.018}$-BDPO@PVA	303-423	3.7	423	This work
$Tb_{0.80}Eu_{0.20}$BPDA	298-318	1.19	313	6
$Tb_{0.9}Eu_{0.1}$-HPIDC-OX	303-473	0.6	473	7
$Eu_{0.2}Tb_{0.8}$L	40–300	0.15	300	8
$Tb_{0.95}Eu_{0.05}$cpna	25–300	2.55	131	9
$Tb_{0.99}Eu_{0.01}(BDC)_{1.5}\cdot(H_2O)_2$	290-320	0.31	318	10
$Eu_{0.0069}$ $Tb_{0.9931}$-DMBDC	50-200	1.15	200	11
$Tb_{0.9}Eu_{0.1}$-L	303–423	1.75	423	12

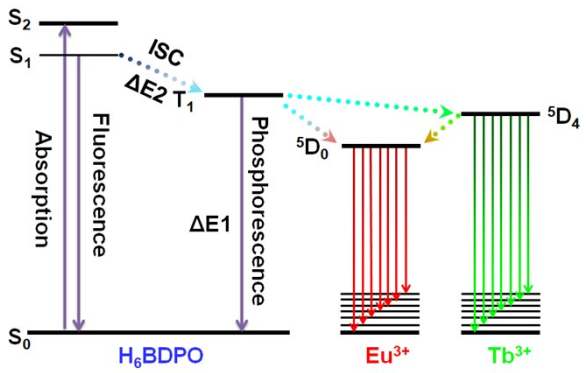

Scheme 1. Schematic representation of the energy adsorption, transfer, and emission processes of Ln-MOF.

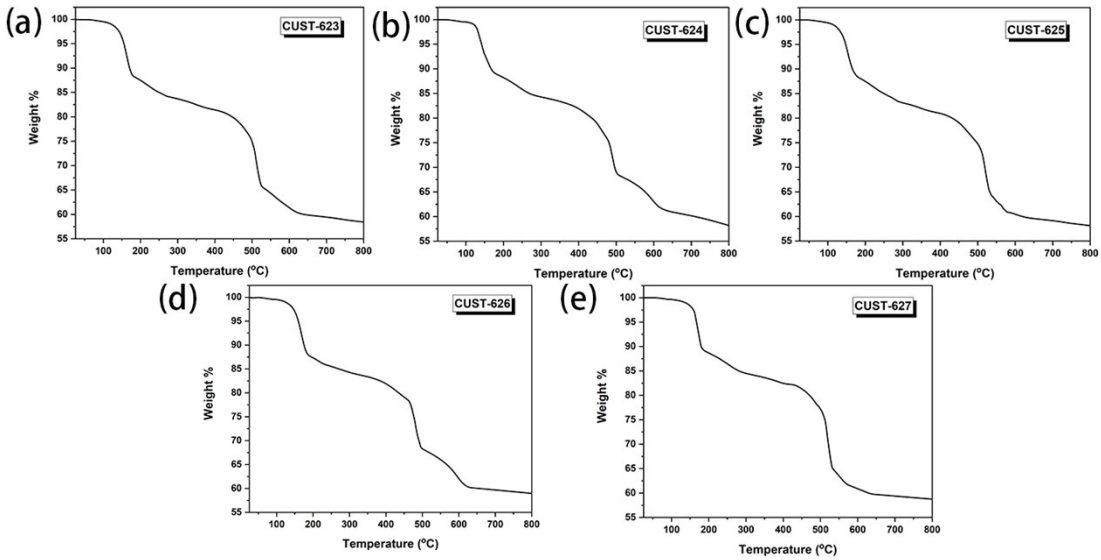

Figure S1. TGA curve of CUST-623 - CUST-627

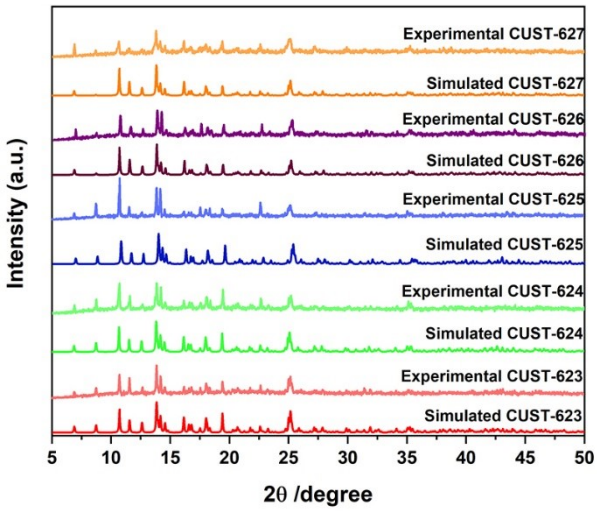

Figure S2. Powder X-ray diffraction patterns of CUST-623 - CUST-627.

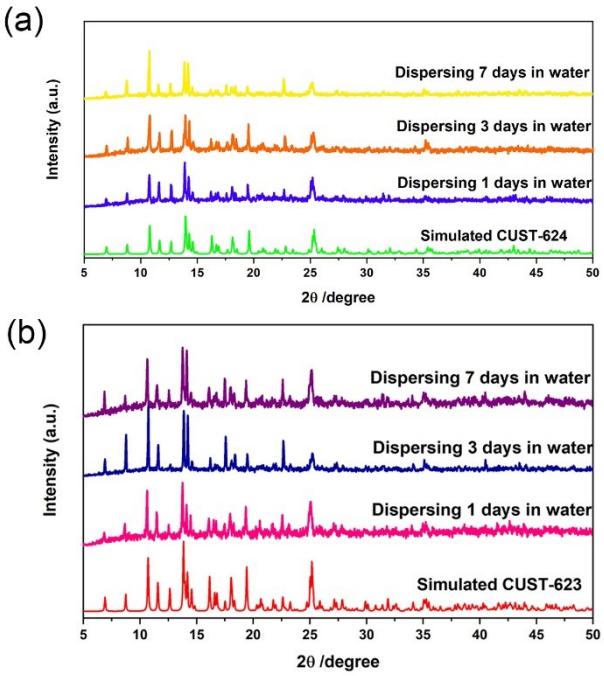

Figure S3. Powder X-ray diffraction patterns of CUST-623 and CUST-624 in water.

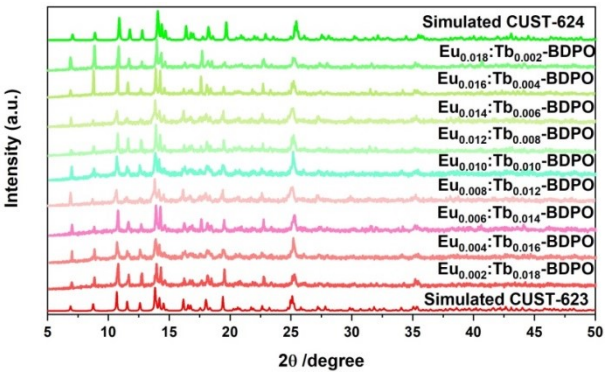

Figure S4. Powder X-ray diffraction patterns of $Eu_xTb_{0.02-x}$- BDPO.

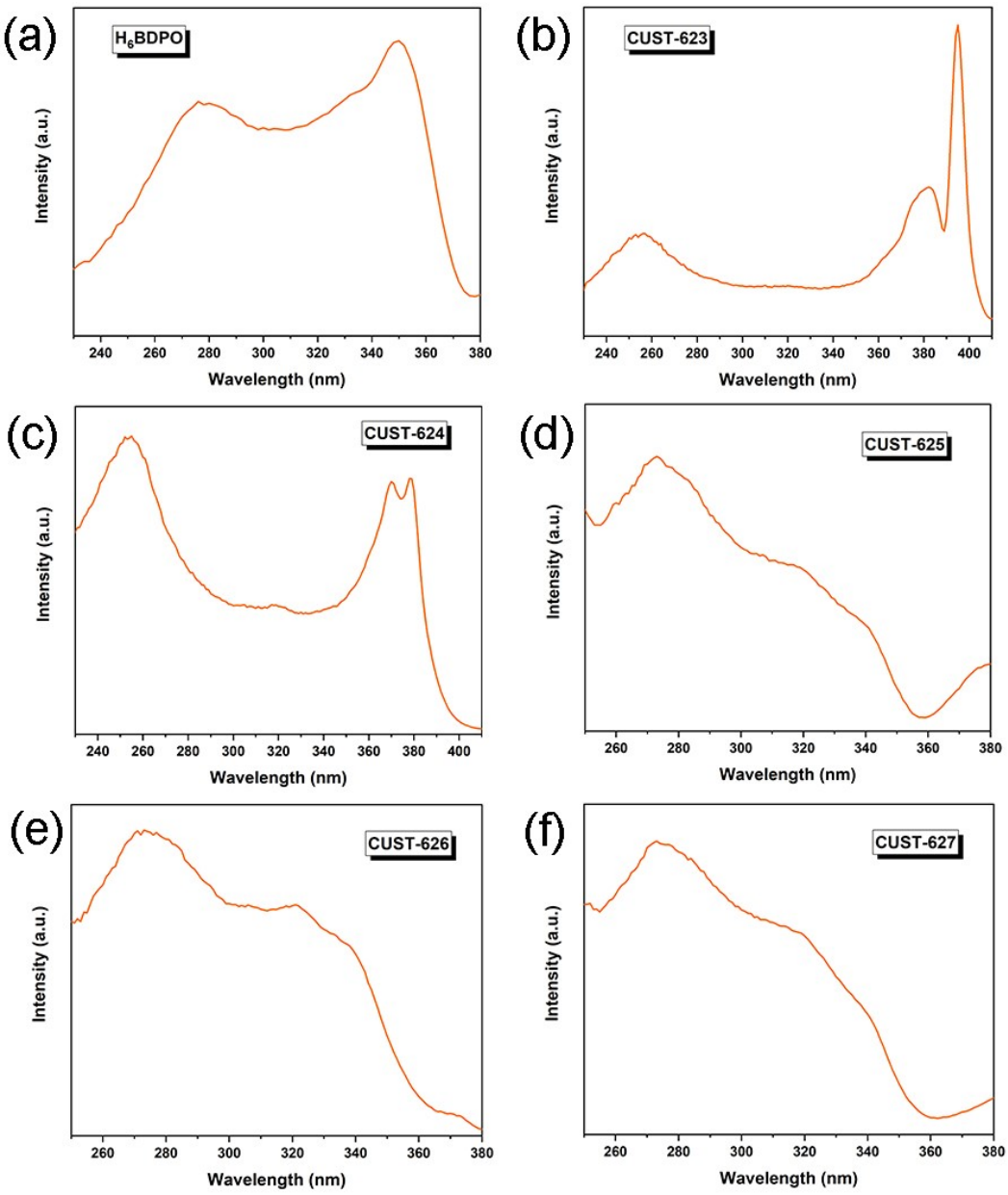

Figure S5. The solid-state excitation spectra H_6BDPO and CUST-623 - CUST-627.

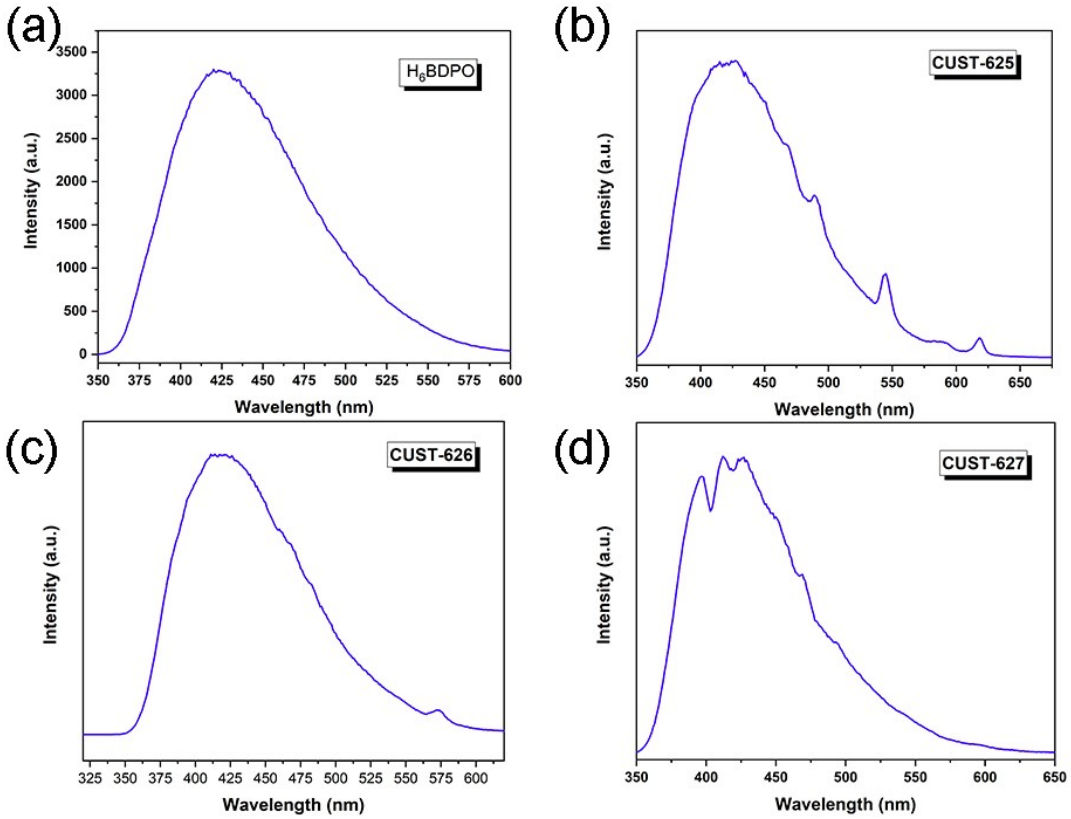

Figure S6. The solid-state emission H_6BDPO and CUST-625- CUST-627

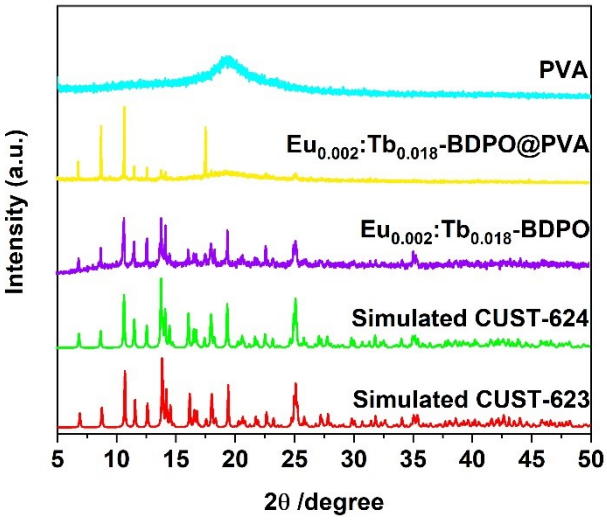

Figure S7. PXRD patterns of $Eu_{0.002}Tb_{0.018}$-BDPO, Polyvinyl Alcohol (PVA), $Eu_{0.002}Tb_{0.018}$-BDPO@PVA membranes and simulated PRXD pattern of Ln-MOFs.

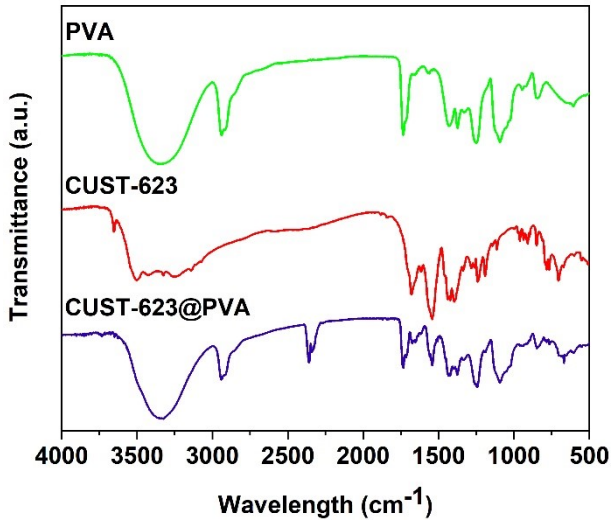

Figure S8. FTIR spectra of Ln-MOFs, Polyvinyl Alcohol (PVA), Ln-MOF@PVA

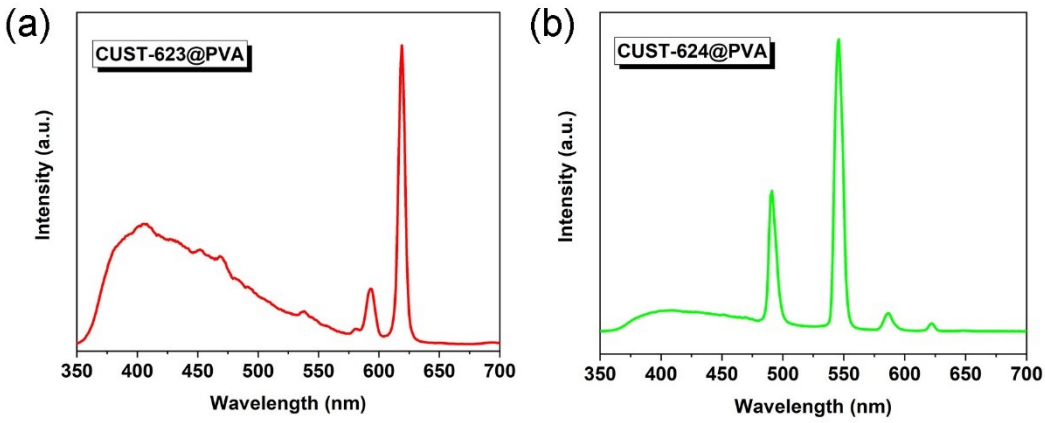

Figure S9. Emission spectra of (a) CUST-623@PVA membrane, (b) CUST-624@PVA membrane

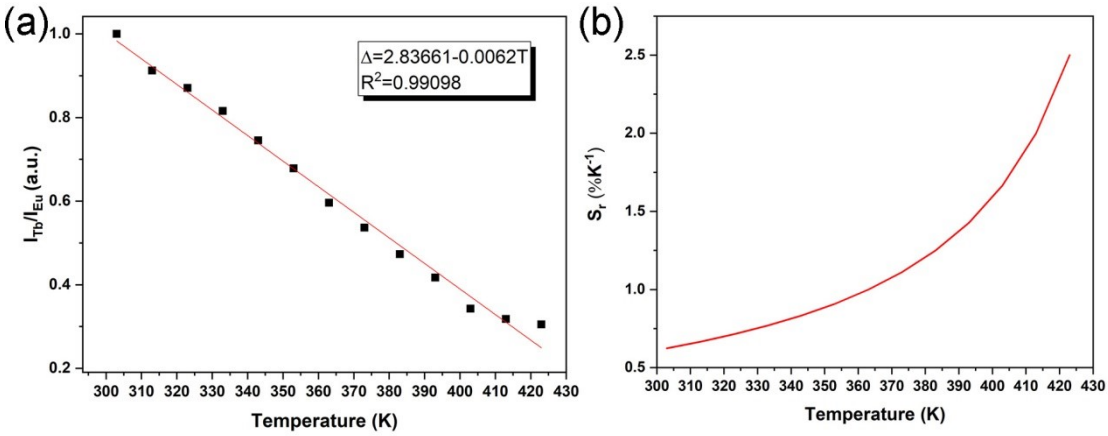

Figure S10. (a) Temperature-dependent intensity ratio of I_{Eu}/I_{Tb} and linearly fitted curve of $Eu_{0.002}Tb_{0.018}$-MOF. (b) The relative sensitivity values (S_r) of $Eu_{0.002}Tb_{0.018}$-MOF.

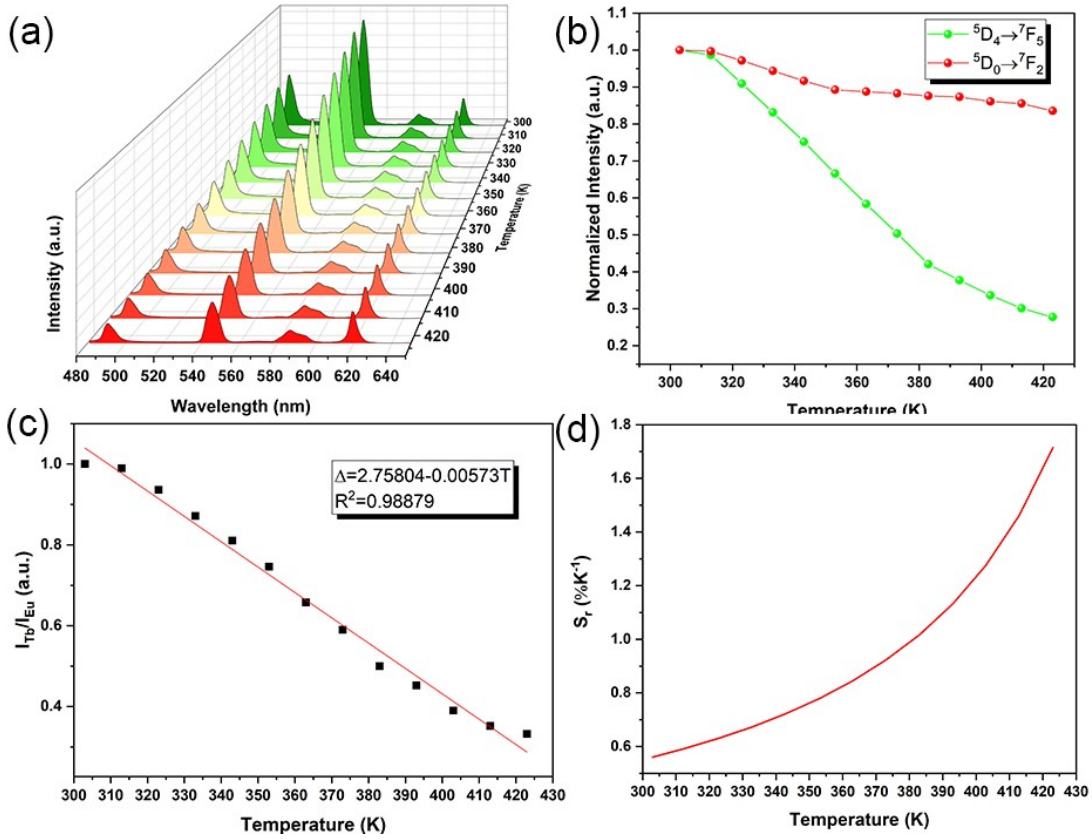

Figure S11. (a) Emission spectra of $Eu_{0.004}Tb_{0.016}$-MOF recorded at 303 K - 423 K. (b) The normalized intensities of $Eu_{0.004}Tb_{0.016}$-MOF. (c) Temperature-dependent intensity ratio of I_{Eu}/I_{Tb} and linearly fitted curve. (d) The relative sensitivity values (S_r) of $Eu_{0.004}Tb_{0.016}$-MOF.

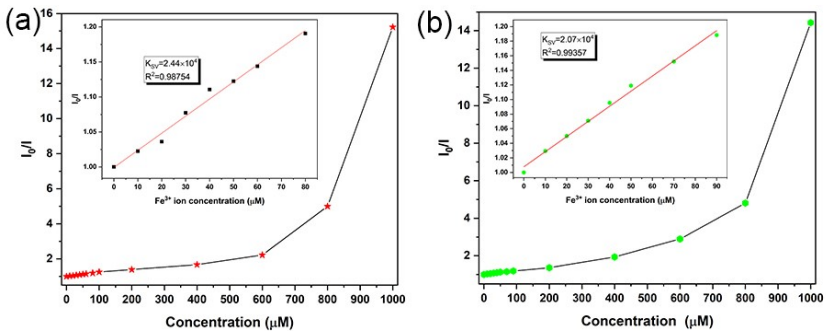

Figure S12. The S−V plot of CUST-623 and CUST-624 of Fe^{3+}.

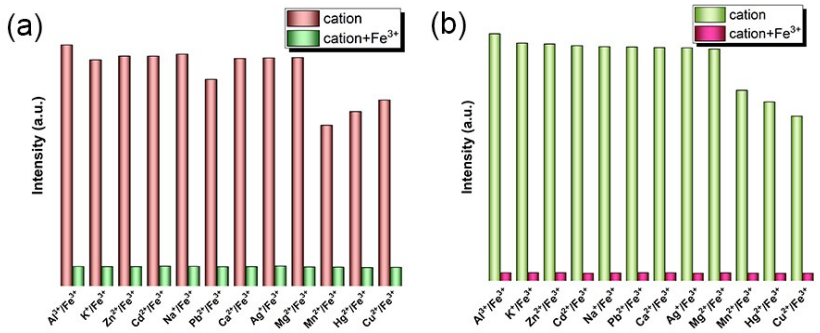

Figure S13. Detect the anti-interference performance spectra of Fe^{3+} ions of CUST-623 (a) and CUST-624 (b).

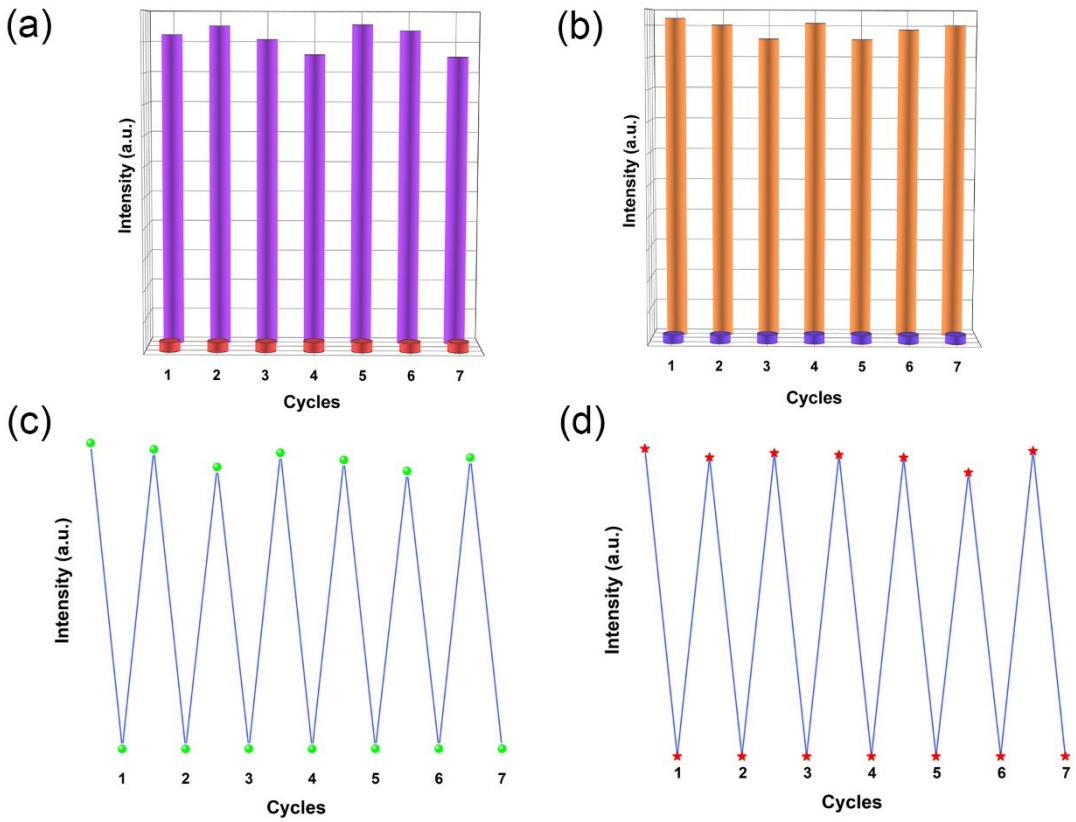

Figure S14. The recovery tests of CUST-623 (a) and CUST-624 (b) in water of $Cr_2O_7^{2-}$ ion. The recovery tests of CUST-623 (a) and CUST-624 (b) in water of CrO_4^{2-} ion.

\

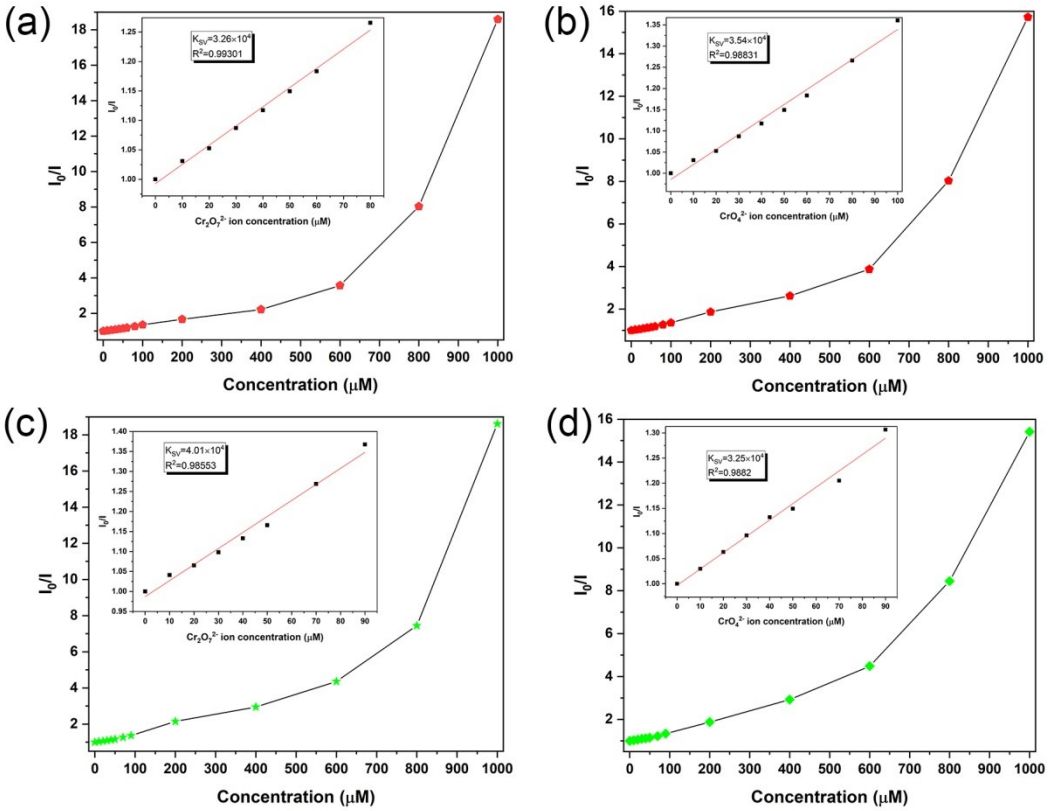

Figure S15. The S−V plot of CUST-623 of (a) $Cr_2O_7^{2-}$ and (b) CrO_4^{2-}. The S−V plot of CUST-624 of (c) $Cr_2O_7^{2-}$ and (d) CrO_4^{2-}. Inset: the linearity relationship of luminescent quenching at low concentrations.

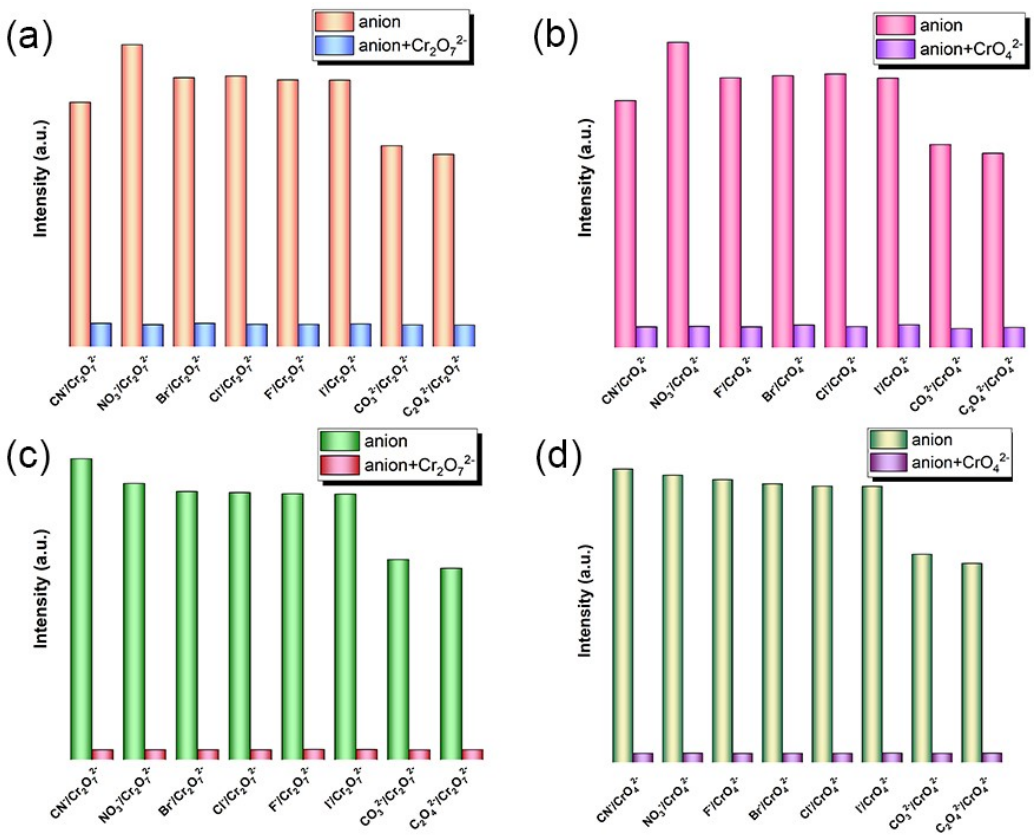

Figure S16. Detect the anti-interference performance spectra of $Cr_2O_7^{2-}$ ions of CUST-623 (a) and CUST-624 (b). Detect the anti-interference performance spectra of CrO_4^{2-} ions of CUST-623 (c) and CUST-624 (d).

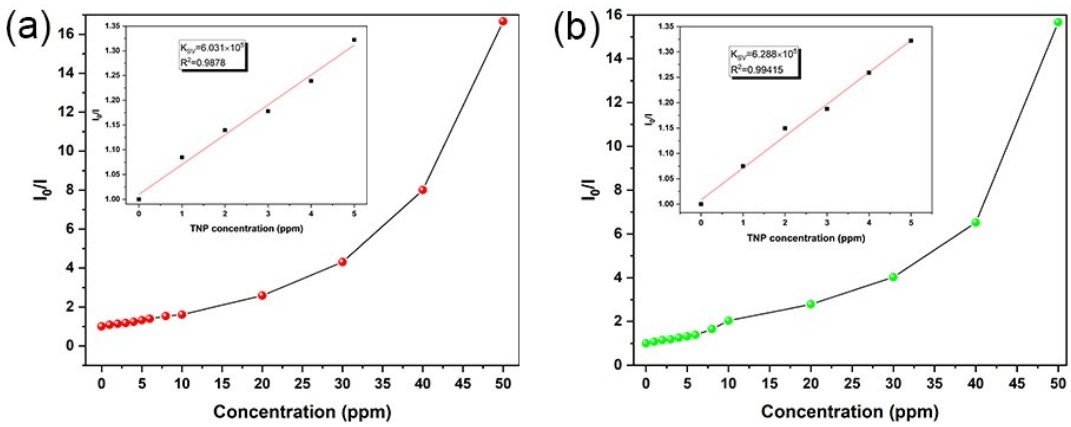

Figure S17. The S−V plot of TNP of (a) CUST-623 and (b) CUST-624. Inset: the linearity relationship of luminescent quenching at low concentrations.

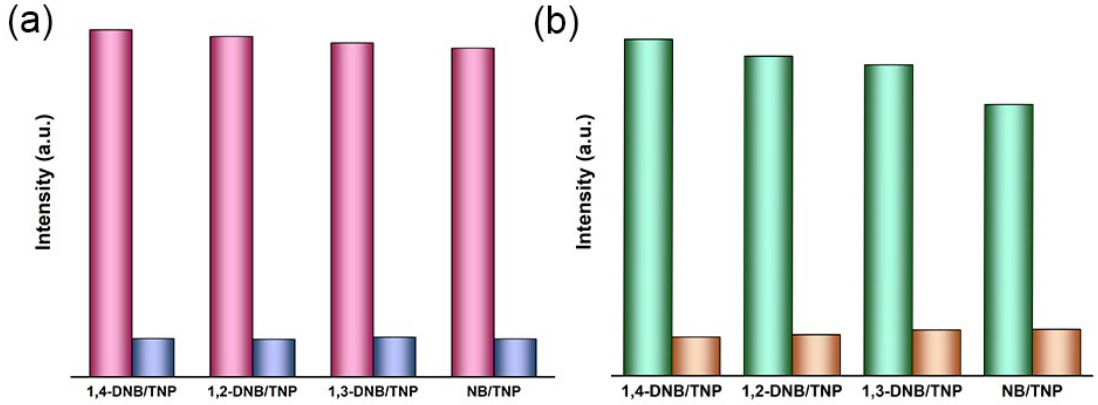

Figure S18. Detect the anti-interference performance spectra of TNP ions of CUST-623 (a) and CUST-624 (b).

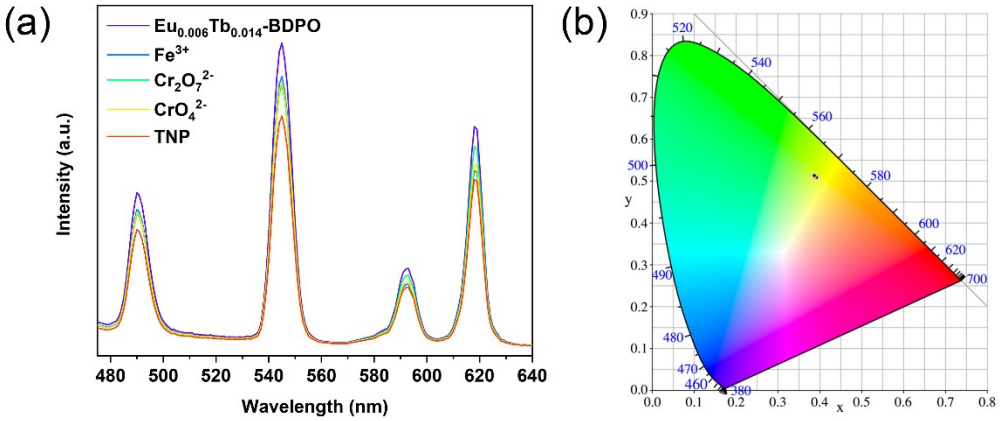

Figure S19. (a) The fluorescence profiles of $Eu_{0.006}Tb_{0.14}$- BDPO after addition of Fe^{3+} (50 μM), $Cr_2O_7^{2-}$ (50 μM), CrO_4^{2-} (50 μM), TNP(5 ppm). (b) CIE coordinates for the response of $Eu_{0.006}Tb_{0.14}$- BDPO to analytes.

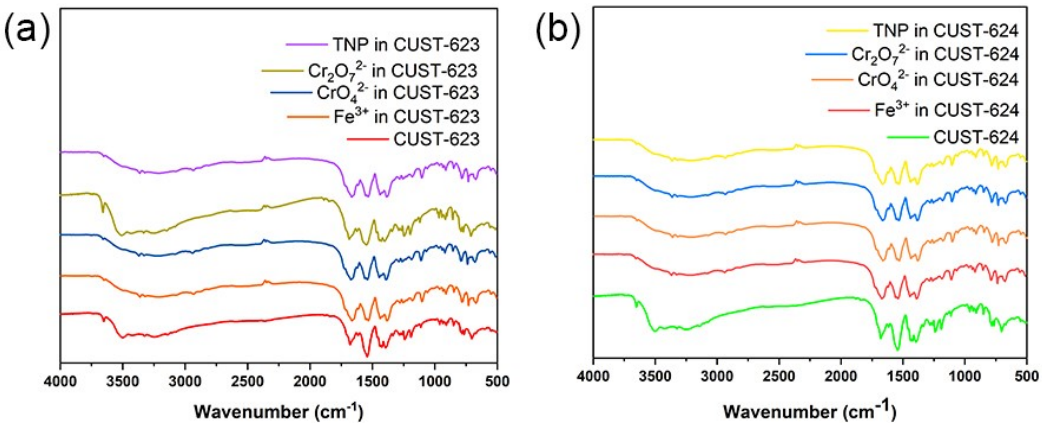

Figure S20. IR spectra of CUST-623 (a) and CUST-624 (b) in different solution.

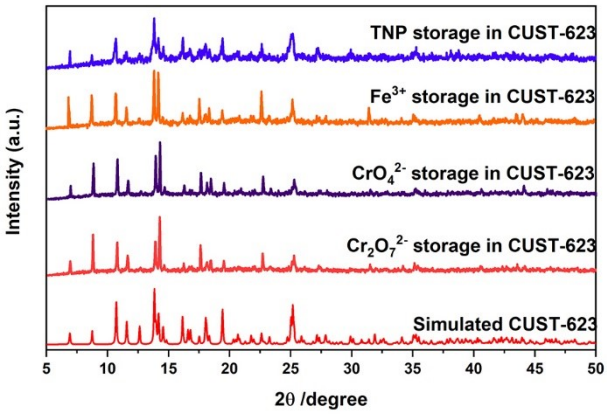

Figure S21. PXRD patterns of CUST-623 after storage Fe^{3+}, $Cr_2O_7^{2-}$, CrO_4^{2-}, TNP.

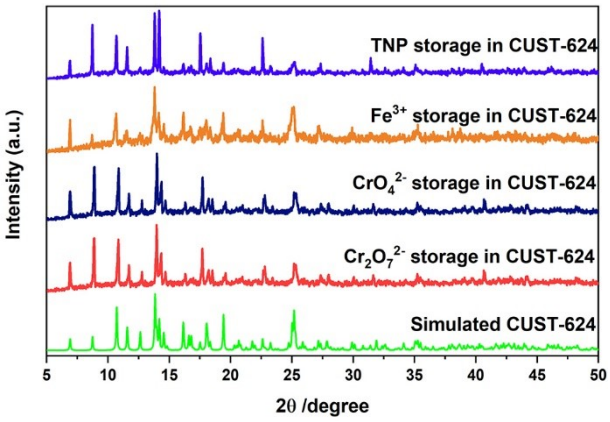

Figure S22. PXRD patterns of CUST-624 after storage Fe^{3+}, $Cr_2O_7^{2-}$, CrO_4^{2-}, TNP.

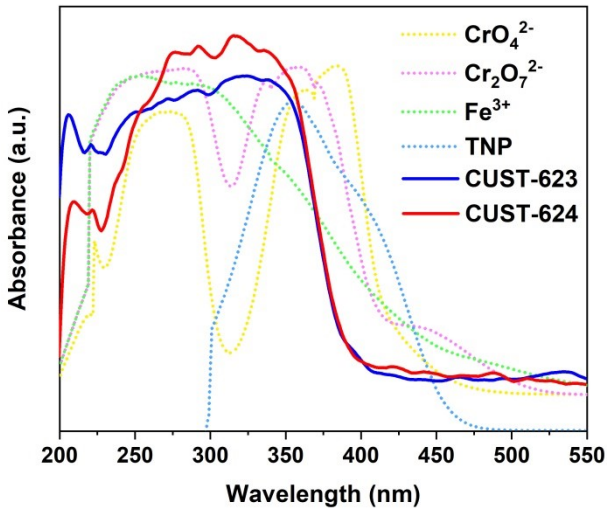

Figure S23. The UV-vis absorption spectra of CUST-623, CUST-624 and TNP, Fe^{3+}, $Cr_2O_7^{2-}$, CrO_4^{2-} ions in water.

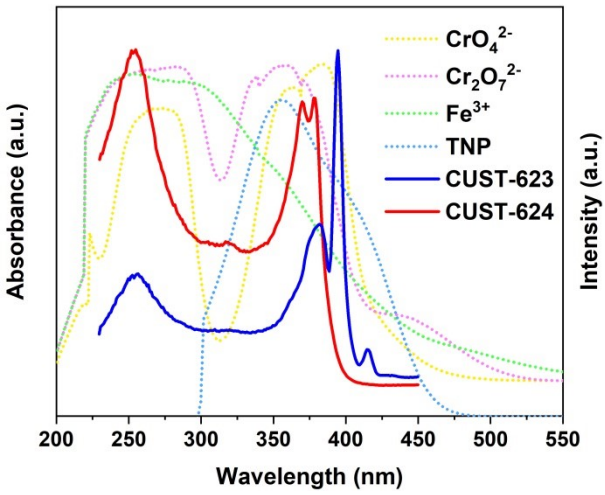

Figure S24. The UV-vis absorption spectra of TNP, $Cr_2O_7^{2-}$, CrO_4^{2-}, Fe^{3+} and the excitation spectra of CUST-623 and CUST-624.

3. Supporting References

1 X. Y. Li, W. J. Shi, X. Q. Wang, L. N. Ma, L. Hou, Y. Y. Wang, Luminescence modulation, white light emission, and energy transfer in a family of lanthanide metal–organic frameworks based on a planar π-conjugated ligand. *Cryst. Growth Des.,* 2017, **17**, 4217-4224.

2 G. M. Sheldrick, A short history of SHELX. *Acta Crystallogr. Sect. A: Found. Crystallogr.,* 2008, **64**, 112−122.

3 S. S. Nagarkar, B. A. K. Joarder, S. Chaudhari, Mukherjee and S. K. Ghosh, Highly selective detection of nitro explosives by a luminescent metal-organic framework. *Angew. Chem. Int. Ed.,* 2013, **52**, 2881-2885

4 M. Y. Fan, H. H. Yu, P. Fu, Z. M. Su, X. Li, X. L. Hu, Q. Q. Pan, Luminescent Cd (II) metal-organic frameworks with anthracene nitrogen-containing organic ligands as novel multifunctional chemosensors for the detection of picric acid, pesticides, and ferric ions. *Dyes Pigm*., 2021, **185**, 108834.

5 E. J. McLaurin, L. R. Bradshaw, D. R. Gamelin, Dual-emitting nanoscale temperature sensors. *Chem. Mater.*, 2013, **25**, 1283-1292.

6 Y. Cui, H. Xu, Y. Yue, Z. Guo, J. Yu, Z. Chen, B. Chen, A luminescent mixed-lanthanide metal–organic framework thermometer. *J. Am. Chem. Soc.,* 2012, **134**, 3979-3982.

7 Y. Yang, H. P. Huang, Y. Z. Wang, F. Z. Qiu, Y. Feng, X. R. Song, X. L. Tang, G. L. Zhang, W. S. Liu, A family of mixed-lanthanide metal-organic frameworks thermometer in a wide temperature range. *Dalton Trans.,* 2018, **48**, 13384-13390

8 H. Wang, J. Xu, D. S. Zhang, Q. Chen, R. M. Wen, Z. Chang, X. H. Bu, Crystalline Capsules: Metal–Organic Frameworks Locked by Size-Matching Ligand Bolts. *Angew. Chem. Int. Ed.,* 2015, **54**, 5966-5970.

9 X. Lian, D. Zhao, Y. Cui, Y. Yang, G. Qian, A near infrared luminescent metal–organic framework for temperature sensing in the physiological range. *Chem. Comm.,* 2015, **51**, 17676-17679.

10 S. N. Zhao, L. J. Li, X. Z. Song, M. Zhu, Z. M. Hao, X. Meng, H. J. Zhang, Lanthanide ion codoped emitters for tailoring emission trajectory and temperature sensing. *Adv. Funct. Mater.,* 2015, **25**, 1463-1469.

11 D. Zhao, D. Yue, K. Jiang, L. Zhang, C. Li, G. Qian, Isostructural Tb^{3+}/Eu^{3+} co-doped metal–organic framework based on pyridine-containing dicarboxylate ligands for ratiometric luminescence temperature sensing. *Inorg. Chem.,* 2019, **58**, 2637-2644.

12 Y. Yang, Y. Wang, Y. Feng, X. Song, C. Cao, G. Zhang, W. Liu, Three isostructural Eu^{3+}/Tb^{3+} co-doped MOFs for wide-range ratiometric temperature sensing. *Talanta.,* 2020, **208**, 120354.